Momentum density of vanadium: A reconstruction from two-dimensional positron-annihilation data

L. M. Pecora and A. C. Ehrlich
Naval Research Laboratory (Code 4631), Washington, D.C. 20375-5000

A. A. Manuel, A. K. Singh, and M. Peter
Departement de Physique de la Matière Condensée, Université de Génève, 32 boulevard d'Yvoy, CH-1211 Génève 4, Switzerland

R. M. Singru
Department of Physics, Indian Institute of Technology, Kanpur 208 016, Uttar Pradesh, India
(Received 14 August 1986; revised manuscript received 21 May 1987)

The momentum distribution, $\rho(\mathbf{p})$, in vanadium has been reconstructed from two-dimensional (2D) angular correlation of positron-annihilation radiation (ACPAR) data sets $n^R(p_x,p_y)$. Reconstruction has been performed by using an expansion in terms of cubic harmonics on experimental as well as theoretical data sets $n^R(p_x,p_y)$ for four orientations in V. The effect of statistical errors propagated during the reconstruction is also estimated. The results for $\rho(\mathbf{p})$ reconstructed from experiment are compared with those from theory by examining radial plots of the momentum distribution, 2D surfaces and their contour plots in various (p_x,p_y) planes. A satisfactory agreement is observed in the general structure shown by the experimental and theoretical distributions and the observed structure is analyzed in terms of contributions from different sheets of Fermi surface (FS) of V. The ratio of $\overline{NP}/\overline{NH}$ of the semiaxes of the N-centered ellipsoidal hole FS sheet in V has been determined to be 1.36 from 2D ACPAR experiment, and this value agrees well with the ratio found by other experimental techniques. Present results show that a wealth of information about $\rho(\mathbf{p})$ can be reconstructed from $n^R(p_x,p_y)$ measured for a limited number of orientations.

I. INTRODUCTION

Recently developed experimental techniques for the measurement of two-dimensional (2D) angular correlation of positron-annihilation radiation (ACPAR) have made it possible to study the two-photon momentum distributions (TPMD's) and Fermi surfaces (FS's) of metals and alloys in greater detail than before.[1,2] The results of 2D ACPAR measurements have been compared with results of solid-state theory[3] by using different approaches,[4] including the reconstruction of the Fermi surface directly from the data.[5] The central problem in the analysis of 1D and 2D ACPAR data is how to extract the TPMD, $\rho(p)$, from the measured data

$$n^R(p_z)\int_{-\infty}^{+\infty}\int_{-\infty}^{+\infty}\rho(\mathbf{p})dp_x dp_y \quad (\text{1D data}) \tag{1}$$

and

$$n^R(p_x,p_y)=\int_{-\infty}^{+\infty}\rho(\mathbf{p})dp_z, \quad (\text{2D data}) \tag{2}$$

where $n^R(p_z)$ and $n^R(p_z,p_y)$ are the ACPAR data sets and R represents the rotation of the sample with respect to the laboratory frame which determines the orientation of the sample as well as the axes in the integrals (1) and (2) above. Thus R labels the data uniquely.

The problem of reconstructing the full three-dimensional distribution, $\rho(\mathbf{p})$, from a set of 1D data $n^R(p_z)$ or 2D data $n^R(p_x,p_y)$ is mathematically equivalent to the problem of tomographic analysis encountered in other fields of science.[6] Attempts to reconstruct $\rho(\mathbf{p})$ by using tomographic techniques developed in other fields present some difficulties because the algorithms involved in these techniques require acquisition of ACPAR data for several orientations, R, of the sample. Normal counting rates in the ACPAR experiments are such that one acquires data sets, n^R, for only a few directions, typically two or three, and at the most five or six. The problem of reconstruction of the momentum distributions from measured 1D ACPAR or 1D Compton profile (CP) data has been reviewed by Mijnarends[7] and his method,[8] based on Fourier-Hankel transforms, has been applied to 1D ACPAR and CP data sets from several solids.[7] Another approach based on the Fourier transform of 1D CP data has been proposed by Mueller,[9] Hansen,[10] and Hauser-Hoffman and Weyrich.[11] Whereas the reconstruction scheme due to Mijnarends is operative in the momentum ($\mathbf{p}$) space, the latter schemes involve calculations in the position ($\mathbf{r}$) space. Since all these methods make use of 1D data sets, their successful application, in practice, requires collection of data sets along several crystalline directions to ensure satisfactory convergence.

On the other hand, the two-dimensional nature of the data, $n^R(p_x,p_y)$, obtained with the modern 2D ACPAR machines, offers rich information for each orientation, R, of the sample. Earlier, Majumdar[12] and Howells and Osmon[13] had proposed schemes operative in momentum

space to reconstruct TPMD, $\rho(\mathbf{p})$, from $n^R(p_x,p_y)$, but their methods have not been applied in practice to real data. Recently, standard "filtered back-projection" techniques have been used to reconstruct $\rho(\mathbf{p})$ from $n^R(p_x,p_y)$ data sets for Cu (Ref. 14) and Gd,[15] but these studies have required special sample orientations to take advantage of crystalline symmetry and several data directions to obtain good quality of results. Application of Cormack's[16] method involving series expansion in polar Fourier form have also been used[17–19] for reconstructing $\rho(\mathbf{p})$, but these schemes also suffer from the same problem of limitation to special planes or directions and necessity to collect data along many directions.

Recently, Pecora[20] has proposed a method to reconstruct $\rho(\mathbf{p})$ using spherical harmonics and it can be described as the Fourier (or position-space) version of previous methods[12,13] employed in the momentum space or as a 2D extension of Hansen's method[10,11] for 1D data sets. We present here the results of the reconstruction of TPMD in metallic V from experimental as well as theoretical 2D ACPAR data sets, $n^R(p_x,p_y)$, along four orientations [p_z, the integration axis in Eq. (2)] by using Pecora's method.[20] A preliminary report of this work has been published elsewhere.[21]

The choice of vanadium as a test case for applying the present method of reconstruction was based on several considerations. First, the band structure, FS, and TPMD in a transition metal like V having partially filled $3d$ states are complicated and challenging enough to provide a severe test of any reconstruction scheme. Secondly, the TPMD in V has been calculated using band-structure theory and the results have been analyzed in terms of electronic band structure and FS topology.[22] Lastly, and most importantly, 2D ACPAR data for V have been measured[23] with good enough momentum resolution and counting statistics to offer reliable data for attempting a reconstruction of the TPMD.

The plan of the present paper is as follows. In Sec. II we present a brief outline of the formalism of the present scheme of reconstruction. Some details of the present calculation are provided in Sec. III. The results of the present work are described and discussed in Sec. IV and the conclusions are summarized in Sec. V to show that the present scheme is successful in reconstructing TPMD from the 2D ACPAR data and that it can be extended to obtain valuable information about the FS topology in V.

II. FORMALISM

A detailed account of the present method for the reconstruction of a full TPMD, $\rho(\mathbf{p})$, from the 2D ACPAR data sets, $n^R(p_x,p_y)$, is given elsewhere[20] and we present here only a brief outline for the sake of completeness. We start with the assumption that the TPMD $\rho(\mathbf{p})$ can be expanded in terms of spherical harmonics,[7,11,20]

$$\rho(\mathbf{p})=\sum_{l,m}\rho_{lm}(p)Y_{lm}(\theta_p,\phi_p)\ , \tag{3}$$

where $p=|\mathbf{p}|$, (θ_p,ϕ_p) are the polar angles of $\mathbf{p}$, and $\rho_{lm}(p)$ are the expansion coefficients which are treated as unknowns in the present scheme. To exploit advantages of working in the position (r) space one can expand[20] $\sigma(\mathbf{r})$, the Fourier transform of $\rho(\mathbf{p})$, in terms of spherical harmonics and write

$$\sigma(\mathbf{r})=\mathcal{F}_{-3}[\rho(\mathbf{p})]=\sum_{l,m}\sigma_{lm}(r)Y_{lm}(\theta,\phi)\ , \tag{4}$$

where $r=|\mathbf{r}|$, (θ,ϕ) are the polar angles of $\mathbf{r}$, and $\sigma_{lm}(r)$ are the unknown coefficients (in the position space) which have to be determined during the reconstruction. By using the well-known Hankel transform one can write

$$\rho_{lm}(p)=\frac{i^l}{2\pi^2}\int_0^\infty j_l(pr)\sigma_{lm}(r)r^2dr\ , \tag{5}$$

where j_l's are the spherical Bessel functions. It is clear that if one can obtain $\sigma_{lm}(r)$ from the experimental data sets, $n^R(p_x,p_y)$, one can determine $\rho_{lm}(p)$ and then reconstruct the full TPMD, $\rho(\mathbf{p})$, through Eq. (3).

Determination of $\sigma_{lm}(r)$ is carried out by following procedure. In the first stage we take a 2D Fourier transform, $\sigma^R(x,y)$, of the 2D ACPAR data sets by writing

$$\sigma^R(x,y)=\int dp_x\int dp_y\, n^R(p_x,p_y)\exp[-i(xp_x+yp_y)]\ . \tag{6}$$

Next we invoke the well-known "central slice" theorem[6] which states that $\sigma^R(x,y)$, the Fourier transform of the data $n^R(p_x,p_y)$, is equal to $\sigma(\mathbf{r})$ on planes in position ($\mathbf{r}$) space which go through the origin ($\mathbf{r}=\mathbf{0}$) and are oriented such that their normal is obtained from the original z axis by rotating by R. This is achieved by expanding $\sigma(\mathbf{r})$ in spherical harmonics whose polar angles are measured relative to the rotated system (x,y,z). Such a rotation from a coordinate system (ξ,ψ,ζ) attached to the sample to that in the laboratory system (x,y,z) can be performed by using the well-known $D^l_{m'm}(R)$ coefficients[7] so that

$$\sigma(\mathbf{r})=\sum_{l,m',m}D^l_{m'm}(R)Y_{lm}(\theta',\phi')\sigma_{lm}(r)\ , \tag{7}$$

where the expansion coefficients $D^l_{m'm}(R)$ depend on the Euler angles of the rotation R and $Y_{lm}(\theta',\phi')$ are the spherical harmonics in the (x,y,z) system.

Since the information $\sigma^R(x,y)$ in Eq. (6) is available in the xy plane, we can set $z=0$ (i.e., $\theta'=90°$) in Eq. (7) and take the Fourier *polar* transform with respect to $\exp(ij\phi')$ of both sides of the equation. This serves to find the jth polar Fourier coefficient of the expression. This operation is possible for the left-hand side because the values are known from the Fourier transform of the data, while the right-hand side can be computed because the spherical harmonics can be expressed in terms of the associated Legendre polynomials and an exponential term:

$$Y_{lm'}(\pi/2,\phi')=P_{lm'}(0)\exp(im'\phi')\ .$$

It has been shown elsewhere[20] that these steps lead to the following system of linear equations involving $\sigma_{lm}(r)$,

$$\sigma^R_j(r)=\sum_{l,m}D^l_{jm}(R)\bar{P}_{jm}(0)\sigma_{lm}(r)\ , \tag{8}$$

where $\bar{P}_{lm}(0)$ are the normalized associated Legendre polynomials and $\sigma_j^R(r)$ are the polar Fourier coefficients of $\sigma^R(x,y)$ obtained from the $n^R(p_x,p_y)$ with the help of Eq. (6). The above system of Eq. (8) can be solved for $\sigma_{lm}(r)$ by choosing a cutoff value $j=l_{\max}$.

The above procedure was tested by using data sets generated from a model with cubic symmetry and consisting of spheres and these results are reported elsewhere.[20] These model calculations have shown that in many cases $l_{\max}$ can be quite large, allowing the solution of coefficients $\rho_{lm}(p)$ for l values of the order of 20–40, even though data sets are available only for a few (2–5) directions. Our results for V presented in Sec. IV support this conclusion. It has been pointed out[11] that high l and m in $\bar{P}_{lm}$ and a large number of terms in Eq. (3) are desirable for reconstruction based on high-angular-resolution data.

In the case of reconstruction of $\rho(\mathbf{p})$ which is invariant under the operations of some point group it is enough to substitute the harmonics associated with the symmetry group in the foregoing equations.[7] For cubic symmetry, as in the case of V, we can write

$$\rho(\mathbf{p})=\sum_k \rho_k(p)K_k(\theta_p,\phi_p)\ , \tag{9}$$

where $K_k(\theta_p,\phi_p)$ are the cubic harmonics[24] such that

$$K_k(\theta_p,\phi_p)=\sum_{l,m} A_{k,lm}\,Y_{lm}(\theta_p,\phi_p) \tag{10}$$

and the coefficients $A_{k,lm}$ are chosen so that the K_k remain invariant under the operation of the proper symmetry point group. This procedure has the advantage of eliminating any Y_{lm} which does not have the proper symmetry and thus enables one to reduce the dimension of the matrix involved while retaining a large $l_{\max}$ value. The remaining equations follow directly from Eqs. (4), (5), (7), and (8) with σ_k replacing σ_{lm} and another summation variable, k, being added to all sums. In this latter case l depends on k.

III. CALCULATIONS

In this section we give some details of the calculations involved in the present reconstruction using the formalism described in the preceding section. In order to examine the reliability of the present reconstruction scheme and to make a proper comparison between experiment and theory we generated theoretical data sets, $n^R(p_x,p_y)$, from theoretical band-structure calculations and put them through our reconstruction scheme. In addition, we have compared the reconstructed TPMD, $\rho(\mathbf{p})$, with that calculated theoretically (but not subjected to reconstruction).

A. 2D ACPAR for V used for reconstruction

Experimental data sets $n^R(p_x,p_y)$ used in the present reconstruction were collected at a temperature of 4.2 K with a high-resolution (0.041×0.068 a.u.^{2}) apparatus using two high-density proportional chambers[25] and single crystals of metallic V. Data sets were measured for four crystal orientations having the p_z (or the integration axis) along [110], [100], [111], and [112] directions and consisted of about 6×10^7 total counts for each orientation. Treatment of the samples and their lifetime measurements showed that the samples were almost free from defects. Details of these measurements and treatment of data are described elsewhere.[23]

Theoretical data sets, $n^R(p_x,p_y)$, for the above four orientations were generated by using Eq. (2) in which the TPMD, $\rho(\mathbf{p})$, was obtained from our previous band-structure calculations[23] [in the independent-particle model (IPM)] for metallic V. Theoretical results of the band structure, FS, and TPMD obtained in these calculations have already been reported in detail earlier.[23] A critical comparison of these theoretical results, including that for $n^R(p_z)$ and $n^R(p_x,p_y)$, with other theoretical and experimental results has already shown[23] that although the theoretical $\rho(\mathbf{p})$ has been calculated by using the fast approximation scheme of Hubbard[26] and Mijnarends,[27] it provides a satisfactory basis to compare experiment with theory. It should be pointed out that the theoretical $\rho(\mathbf{p})$ and $n^R(p_x,p_y)$ calculated from it and used in the present work did not include contributions from the core $(1s)^2(2s)^2(2p)^6(3s)^2(3p)^6$ electrons, and nor were any corrections for the e^--e^- and e^+-e^- many-body correlations (so-called enhancement effects) applied. It has already been shown[23] that the contribution from the core electrons is already small and that it has to be reduced by a factor $\alpha=0.2$–0.3 to obtain a satisfactory agreement between experiment and theory. The theoretical 2D ACPAR curves, $n^R(p_x,p_y)$, were convoluted with the angular resolution of the apparatus before subjecting them to the reconstruction procedure.

B. Working details of the reconstruction calculations

The cubic symmetry versions given in Eqs. (9) and (10) were used to solve for $\rho_k(p)$, the coefficient of the kth cubic harmonic for both the experimental data and the theoretically generated data (hereinafter called theoretical data). It is necessary to invert a matrix when solving Eq. (8). The numerical stability of this matrix inversion (as in many other problems involving matrix inversion) depends on the dimension of the matrix, the instability usually increasing with the dimensions due to computer round-off error, as well as the existence of small eigenvalues of the matrix. The dimension above which the matrix cannot be inverted on a computer (64-bit double precision) determines the upper bound for the cutoff, $k_{\max}$.

It has been shown[20] that Eq. (8) generates a particularly stable matrix for many situations which can be inverted up to large dimensions. In the present reconstruction calculations using data sets, $n^R(p_x,p_y)$, for four orientations of V we were able to solve for $\rho_k(p)$ for $k_{\max}=40$. However, we found that the structure of the reconstructed $\rho(\mathbf{p})$ did not change significantly when terms with $k>25$ were included in the expansion. In view of this result, we limited to k to $k_{\max}=25$ in all the reconstruction calculations presented here. This corresponds to a maximum value of $l=30$ and an angular resolution of 6°.

The reconstruction of the experimental data was

smoothed by modulating the solutions in the position space by a Gaussian "window" which was equivalent to convoluting the data with a 2D Gaussian in momentum space having a full width at half maximum (FWHM) of 0.04 a.u. (0.3 mrad) in each direction. This smoothing did not change the reconstruction significantly, except for $p < 0.3$ a.u., where it helped to suppress the usual fluctuations present in the reconstructions near the origin. Although these fluctuations were small in our case we felt that in view of the estimated error (see below) they distorted the real structure present. Combining the above convolution with the experimental resolution gives a radial resolution about 0.053 a.u. (or 0.4 mrad).

The reconstruction of the theoretical $\rho(\mathbf{p})$ from the theoretical data was handled in the same way, except in this case we smoothed the reconstruction with a Gaussian of FWHM equal to 0.069 a.u. (0.5 mrad) to obtain a better matching with the reconstruction of experimental data. Our tests showed that inclusion of TPMD due to core electrons made little difference in the TPMD reconstructed from experiment and theory.

In order to estimate the propagation of statistical errors in the data by the present reconstruction scheme we generated random log-normal-distribution error data arrays consistent with the number of counts in each data projection.[20] We put several such sets through the reconstruction programs. The statistical errors in the resulting reconstructions showed a strongly isotropic distribution in momentum space. We, therefore, calculated a spherical average of the square of the error at several radial distances. The square root of this average is plotted in Fig. 1 as a function of radial (momentum p) distance. The units of the error (ordinates in Fig. 1) are the same as the units in all subsequent plots of the $\rho(\mathbf{p})$ values to be presented in Sec. IV and thus allow a direct comparison of the absolute error expected in reconstruction of the experimental data with the size of the structure present at each radial distance.

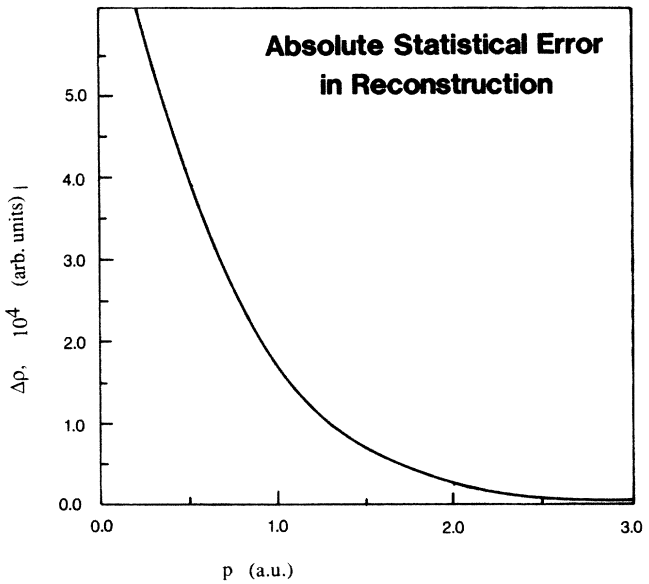

FIG. 1. Statistical error ($\Delta\rho$) expected in the present reconstruction scheme as a function of momentum (see text). The units of $\Delta\rho$ are the same as that of $\rho(\mathbf{p})$ in the subsequent plots shown in Figs. 2–5.

IV. RESULTS OF THE RECONSTRUCTIONS AND THEIR DISCUSSION

As mentioned in Sec. III the results of our theoretical calculation of electron band structure, positron wave function, FS topology and TPMD, $\rho(p)$, for V have been described in previous reports.[23] Our present results for reconstructed $\rho(\mathbf{p})$ can be better understood in terms of the three different sheets of FS for V: (i) second-band octahedral hole surface centered at Γ ["Γ-centered, octahedral" (GCO)], (ii) third-band distorted ellipsoidal hole surface centered at N ["N-centered, ellipsoidal" (NCE)], and (iii) third-band multiply connected "jungle-gym" arms along the $\langle 100 \rangle$ directions ["jungle-gym arms" (JGA's)], where GCO, NCE, and JGA are the labels by which we shall refer to these FS's in our discussion.

Presentation of our results for reconstructed $\rho(\mathbf{p})$ and their comparison is made in different ways. In this discussion we shall refer to three types of distribution for V: (i) $\rho_t(\mathbf{p})$, theoretically calculated[23] (but *not* reconstructed) TPMD due to band electrons, (ii) $\rho_{re}(\mathbf{p})$, TPMD reconstructed from the experimental 2D ACPAR data sets, $n^R(p_x,p_y)$, and (iii) $\rho_{rt}(\mathbf{p})$, TPMD reconstructed from theoretical 2D ACPAR data sets.

Present results for TPMD are shown in Figs. 2–11 in terms of radial plots, 2D surfaces, and contour plots. Comparisons of $\rho_{re}(\mathbf{p})$ and $\rho_{rt}(\mathbf{p})$ versus p along the three symmetry directions $\langle 100 \rangle$, $\langle 110 \rangle$, and $\langle 111 \rangle$ are shown in Figs. 2–4, respectively, along with the statistical error caused by the reconstruction procedure. Also shown in the inset of Figs. 2–4 are the relevant electronic bands which contribute to $\rho_t(p)$ in the first two Brillouin zones (BZ's) along that $\mathbf{p}$ direction and the plot of $\rho_t(\mathbf{p})$ itself. The bandwise contributions to the electron momentum distribution (i.e., for Compton scattering) in V have been analyzed by Kanhere and Singru[28] and a similar analysis for the TPMD has been reported previously.[22]

Before we discuss the special features observed in Figs. 2–4, some comments on the general trends shown by $\rho_{re}(\mathbf{p})$ and $\rho_{rt}(\mathbf{p})$ are in order. First, the radial plots of the reconstructed TPMD in Figs. 2–4 show an oscillatory structure in the region $p < 0.5$ a.u. where the statistical error expected due to the reconstruction process is already high. These oscillations are ascribed to the propagation of correlated noise in the reconstruction. Secondly, we observe that although the experimental and theoretical curves in Figs. 2–6, 8, and 10 show similar structures, the theoretical curves display sharper structures. Similar behavior was observed for $\rho_{re}(\mathbf{p})$ and $\rho_{rt}(\mathbf{p})$ reconstructed for Cu (Refs. 1 and 14) from the 2D ACPAR data. This is an effect which appears to show up in all comparisons of the reconstruction of the experimental TPMD of V versus reconstructions of the theoretical TPMD. Certainly, this might suggest a simple discrepancy between experiment and theory; that is, the

theoretical structures may be larger than they should be. However, in the following detailed discussion of the results we also consider some other possibilities: the many-body correlation effects and the experimental resolution. In particular, much of the structure in the TPMD of V results from the d bands. There is some suggestion that, as a result of many-body interactions, in some transition metals the contribution of d states to the TPMD is *deenhanced* relative to the s and p states,[29] whose contributions are usually enhanced, especially near the Fermi level. We note that this mechanism may be in operation here, causing much of the structure to appear smaller than its band-theory counterpart, although this has not been examined in detail. Since the main aim of the present work is to demonstrate the applicability of the reconstruction algorithm described in Sec. II to 2D ACPAR data sets measured for a limited number of orientations, we have not attempted a detailed treatment of many-body correlation effects.

Examination of the distributions shown in Fig. 2 indicate that $\rho_t(\mathbf{p})$, shown in the inset, does not possess much structure along the [100] direction in the first and second BZ's and this behavior is confirmed by $\rho_{re}(\mathbf{p})$ as well as $\rho_{rt}(\mathbf{p})$. However, a slight bulge is observed in $\rho_t(p)$ just beyond the point H in the second BZ. This feature is reproduced by $\rho_{re}(\mathbf{p})$ and $\rho_{rt}(\mathbf{p})$ in the range $p=1.25-1.34$ a.u. with the position of the bulge in $\rho_{re}(\mathbf{p})$ occurring at a slightly lower ($\sim 4\%$) $\mathbf{p}$ value when compared to $\rho_{rt}(\mathbf{p})$. We ascribe this discrepancy to the difference in the lattice parameter a.

It should be noted that our theoretical calculations were based on the crystal potential for V as calculated by Moruzzi *et al.*,[30] who have used the value of $a=5.54$ a.u. corresponding to zero pressure. In order to maintain an internal consistency with their crystal potential we decided to work with the same value, $a=5.54$ a.u., in our calculation of $\rho_t(\mathbf{p})$, although the experimental value was found to be 3.4% higher (i.e., $a=5.726\pm0.006$ a.u.). In the earlier reports,[23] our theoretical results obtained for the energy bandwidths and semiaxes of NCE (FS sheet) in V using $a=5.54$ a.u. have been compared with other theoretical and experimental results to demonstrate satisfactory agreement. The effect of the lattice parameter on TPMD was checked by comparing our results for $\rho_t(\mathbf{p})$ for V with those obtained by Singh and Jarlborg,[31] who made a self-consistent calculation of $\rho_t(\mathbf{p})$ in V for $a=5.726$ a.u. using the linear muffin-tin-orbital method of band structure. This comparison has shown that a 3.4% change in the lattice parameter causes a lateral shift in the position ($\mathbf{p}$ values) of the structure in the $\rho_t(\mathbf{p})$, but the amplitude, shape, and the peak-to-valley ratios in these curves are not affected significantly. The

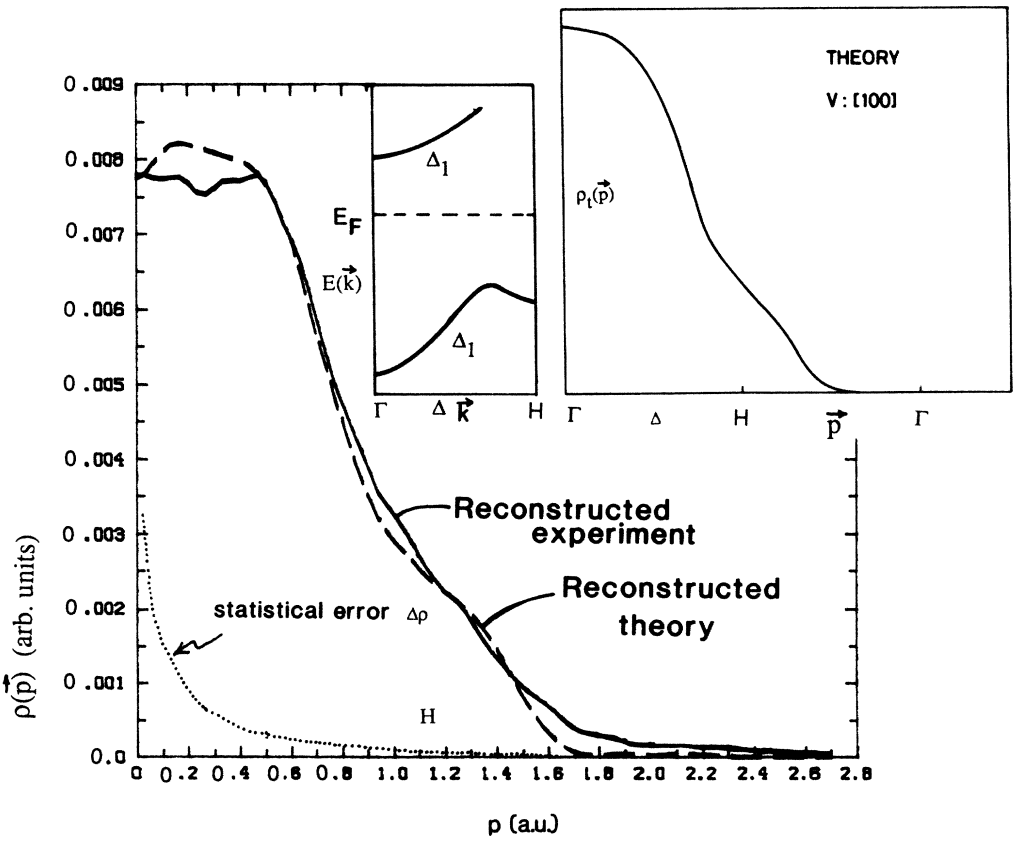

FIG. 2. Reconstructed TPMD $\rho_{re}(\mathbf{p})$ (solid curve) and $\rho_{rt}(\mathbf{p})$ (dashed curve) along the [100] direction in V (see text). The dotted curve indicates the statistical error generated during the reconstruction. The inset shows the relevant band structure $E(k)$ vs k and a plot of $\rho_t(\mathbf{p})$ along $\langle 100\rangle$ (see text).

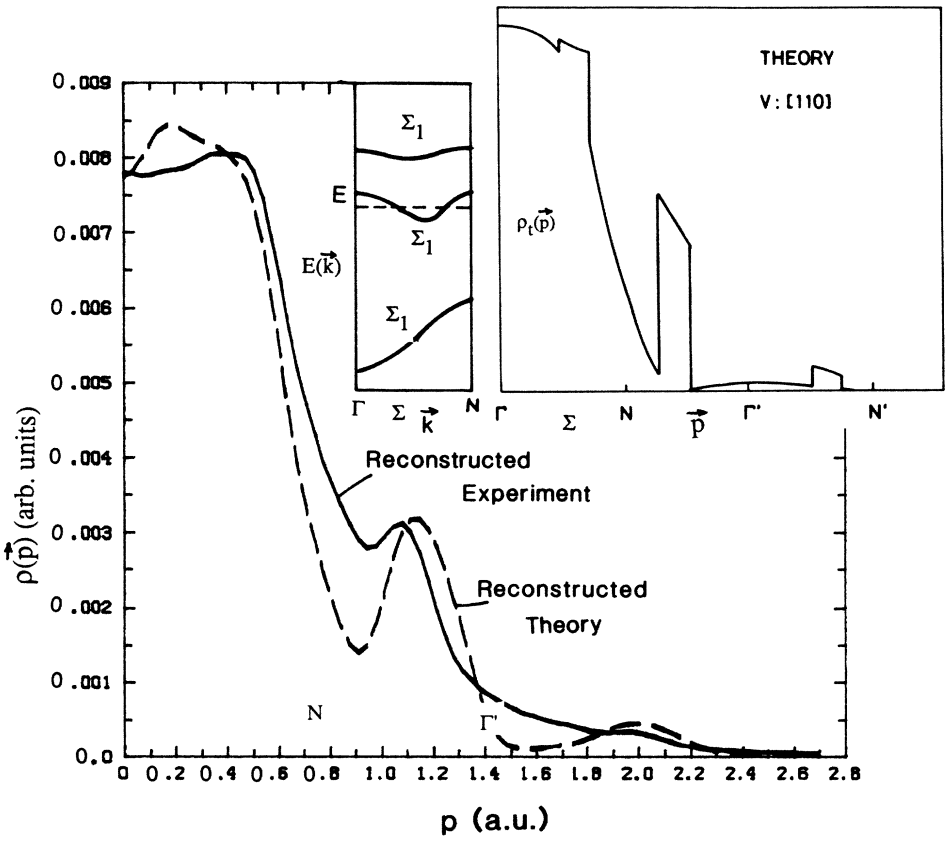

FIG. 3. Same as Fig. 2, but for the [110] direction.

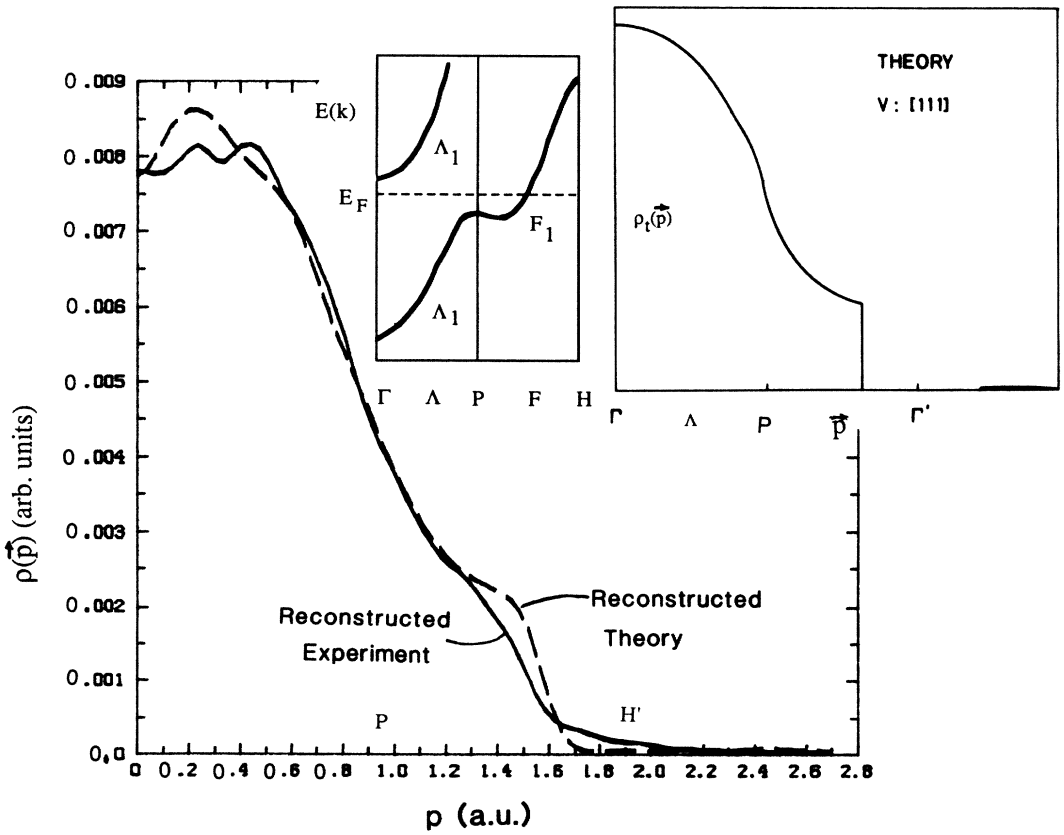

FIG. 4. Same as Fig. 2, but for the [111] direction.

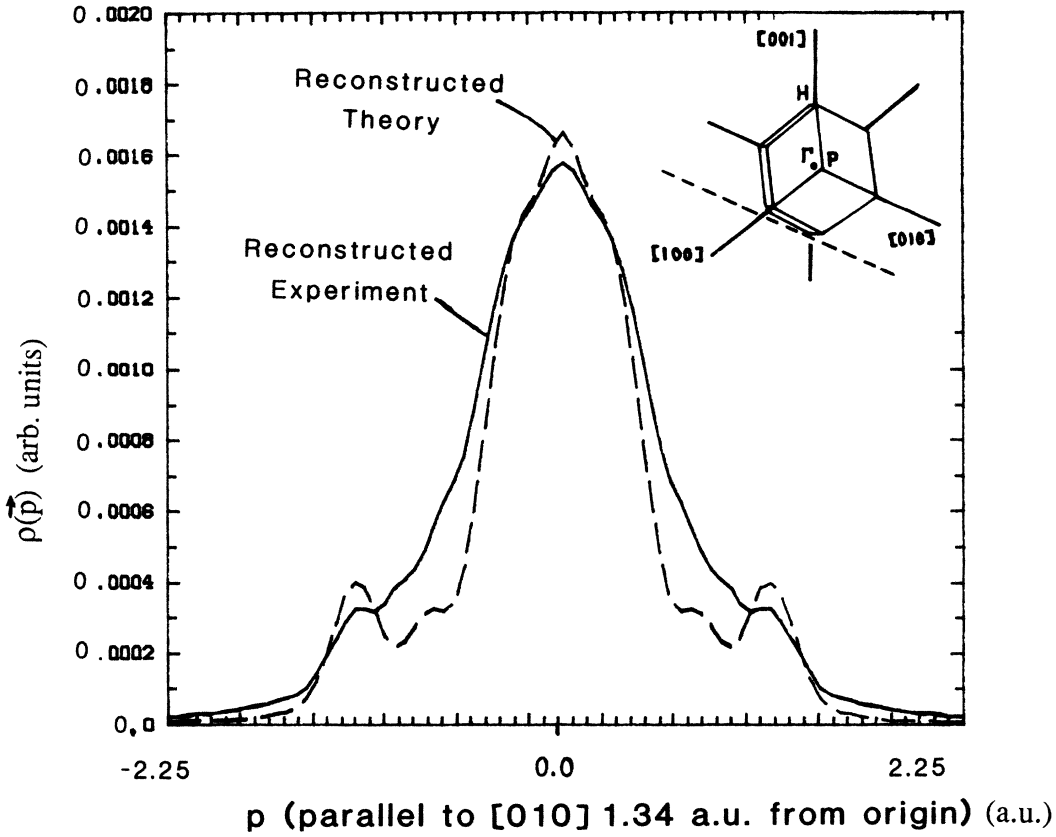

FIG. 5. Reconstructed TPMD $\rho_{re}(\mathbf{p})$ (solid curve) and $\rho_{rt}(\mathbf{p})$ (dashed curve) along a line ($\mathbf{p}$) parallel to [010] and displaced from the origin along [100] by 1.34 a.u. This particular $\mathbf{p}$ line is the dashed line in the Brillouin-zone model shown in the top right corner of the figure. It should be pointed out that the structure observed in both the curves is occurring mainly in the second and third BZ.

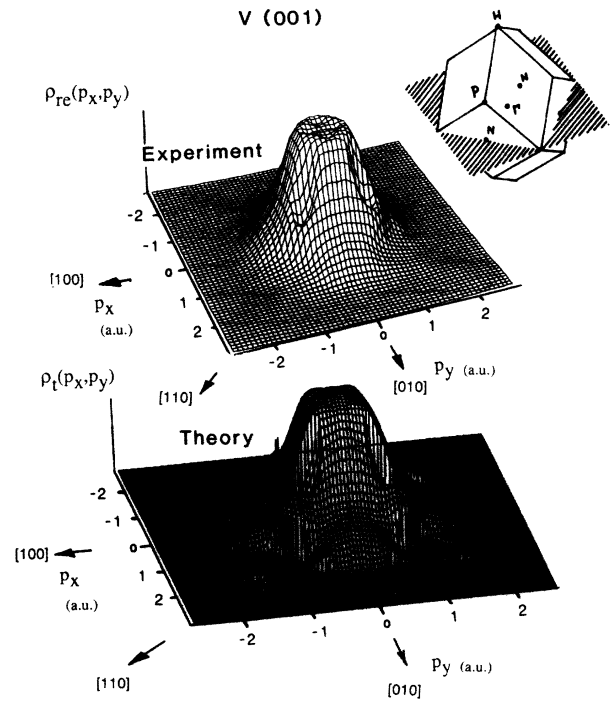

FIG. 6. The TPMD surfaces $\rho_t(p_x,p_y)$ and $\rho_{re}(p_x,p_y)$ (see text) in the $(p_x,p_y)=(001)$ plane passing through Γ at $p_z=0$. The particular (p_x,p_y) plane is shown in the inset at the top right corner.

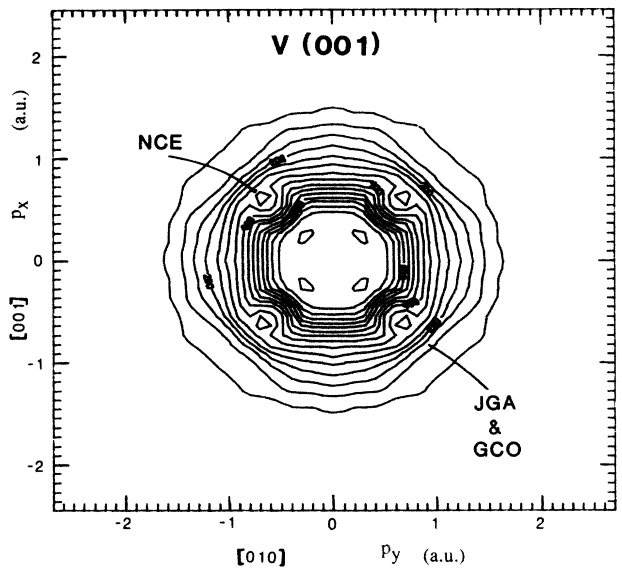

FIG. 7. Contour plot of $\rho_{re}(p_x,p_y)$ shown in Fig. 6 in the particular (p_x,p_y) plane. The labels NCE, JGA, and GCO indicate the effect of the particular sheets of FS of V on the structure observed.

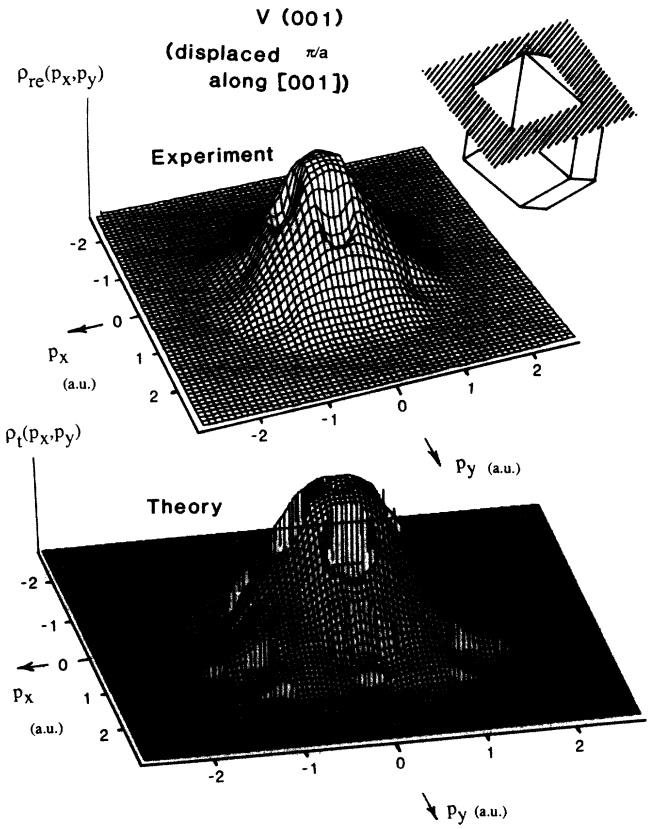

FIG. 8. Same as Fig. 6, but for $(p_x,p_y)=(001)$ situated at $p_z=\pi/a$ along the [001] direction.

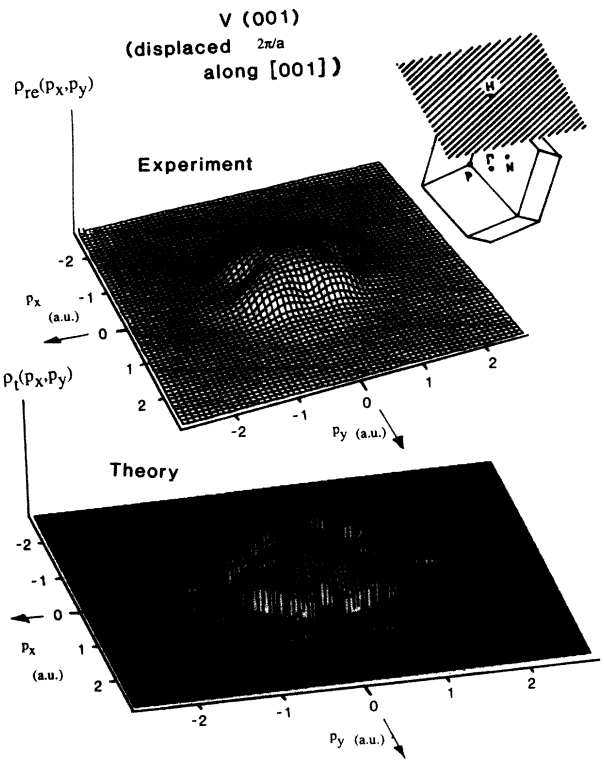

FIG. 10. Same as Fig. 6, but for a $(p_x,p_y)=(001)$ plane situated at $p_z=2\pi/a$ along the [001] direction.

lateral shifts observed between the structures displayed by $\rho_{re}(\mathbf{p})$ and $\rho_{rt}(\mathbf{p})$ curves in Figs. 3 and 4 can thus be attributed to the difference between the theoretical and experimental value of a.

The radial plots of $\rho_t(\mathbf{p})$ along the [110] direction shown in Fig. 3 show very interesting structure which arises from the dipping of the second Σ_1 band below the Fermi level ($E=E_F$) by a few (10–15) mRy between Γ and N. The occupied part of this second Σ_1 band (see inset of Fig. 3) gives rise to "spikes" in the $\rho_t(\mathbf{p})$ curve at $p=0.45$ a.u. and through the umklapp images at $p=1.1$ and 2.0 a.u. as explained elsewhere.[22,28] In the literature,

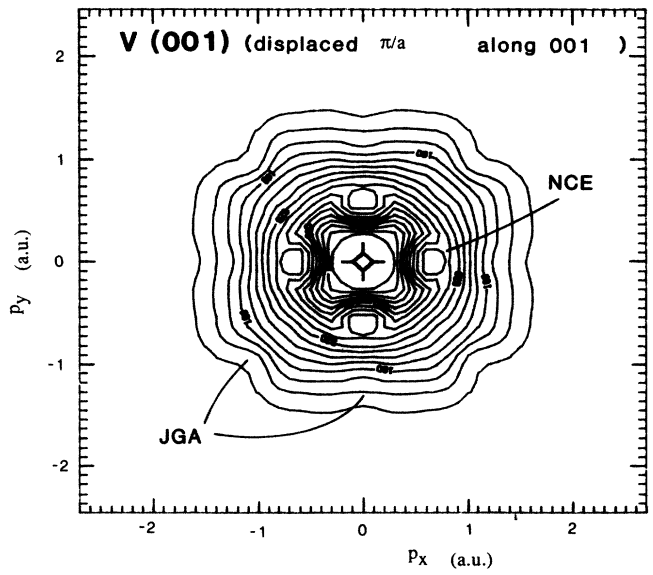

FIG. 9. Contour plot of $\rho_{re}(p_x,p_y)$ shown in Fig. 8 in the particular (p_x,p_y) plane.

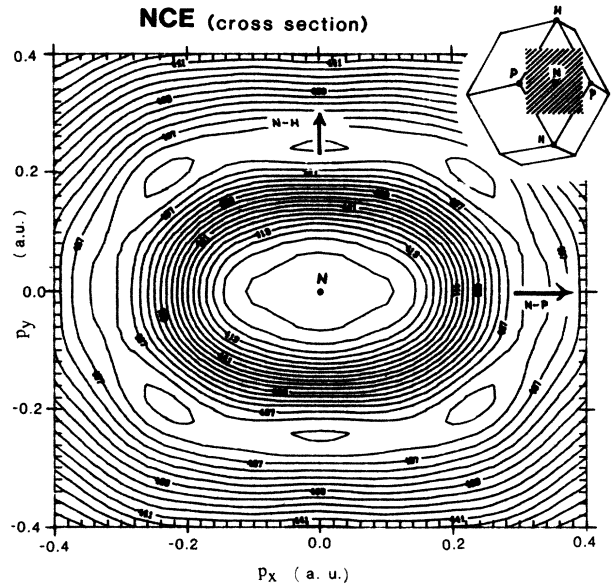

FIG. 11. Contour plot of $\rho_{re}(\mathbf{p})$ in a plane lying in the *HPHP* plane (centered at N) on the face of the first BZ. This particular plane is indicated in the inset of the figure. The *NP* and *NH* axes are also indicated in the figure.

there exists speculation about the existence of narrow necks connecting the JGA and NCE FS sheets in V along the ⟨110⟩ directions. Such necks will appear if the second Σ_1 band lies above $E=E_F$ all along the Σ direction and as a result the spikelike structure in $\rho_t(\mathbf{p})$ should be noticeably absent in V along the [110] direction. The fact that the $\rho_{re}(\mathbf{p})$ plot in Fig. 3 shows a prominent peak at $p\sim 1.1$ a.u. is a strong indication that the second Σ_1 band dips below the Fermi level and that there is *no* neck along ΓN in the FS of V. The structure observed in the $\rho_{re}(\mathbf{p})$ and $\rho_{rt}(\mathbf{p})$ curves (Fig. 3) in the region $p=1.0-1.2$ a.u. reveals two marked differences. First, there is a lateral shift in the positions of this peak which is attributed to the difference in the lattice parameter as pointed out earlier. Secondly, the peak in $\rho_{rt}(\mathbf{p})$ appears more prominent and has a higher "peak-to-valley" ratio compared to $\rho_{re}(\mathbf{p})$. This observed difference between the amplitudes of the $\rho_{re}(\mathbf{p})$ and $\rho_{rt}(\mathbf{p})$ curves could arise from a slight azimuthal misalignment of the sample during measurement. The procedures used permit us to align the sample within ± 1 degree and we estimate that this error is not sufficient to explain the observation. As explained earlier, a 3.4% change in the lattice parameter did not change the amplitudes in $\rho_t(p)$ distributions significantly.[31] We, therefore, feel that the significant differences in the amplitude and peak-to-valley ratios observed in Fig. 3 need some other explanation.

Three possibilities can be suggested to explain the observed behavior. One is that present theory has overestimated the lateral size ($\mathbf{p}$ values) of the drop of the second Σ_1 band below $E=E_F$ in the $E(k)$-versus-k relation along the Σ axis. A second possibility is that the present theory has underestimated the contribution of the first filled Σ_1 band in the region of the valley observed in Fig. 3. Another possibility is that the relative e^+-e^- many-body corrections (i.e., enhancement factors) for the first and second Σ_1 bands are different with the partial contributions to $\rho(\mathbf{p})$ by the second Σ_1 band, which has a $3d$ character and is closer to $E=E_F$, getting *deenhanced.* Recently Singh *et al.*[29] have found evidence in Ni for such a deenhancement of $\rho(\mathbf{p})$ for $3d$ bands near $E=E_F$ and they have proposed a partial enhancement factor $\varepsilon_l(\gamma)$ for each l state. Although an energy-dependent enhancement in $3d$ metals has been suggested earlier,[32,33] the possibility that the enhancement factor for d states is lower than s or p states needs to be further investigated in detail for transition metals in general and for the present experimental data for V in particular.

The plot of theoretical TPMD, $\rho_t(\mathbf{p})$, along the [111] direction shows a sharp discontinuity at about $p=1.55$ a.u. (see inset of Fig. 4) arising out of the crossing of the Λ_1 band (JGA) with the Fermi level along F ($=PH$). This is manifested in the reconstructed curves, $\rho_{re}(\mathbf{p})$ and $\rho_{rt}(\mathbf{p})$, in the form of a shoulder (Fig. 4) in the region $p=1.3-1.5$ a.u., with the experimental curve showing a smoother structure. Once again the weaker character of this structure shown by $\rho_{re}(\mathbf{p})$ could be caused by the deenhancement of the Λ_1 band, which has $3d$ character near E_F.

In Figs. 2–4 we have shown the radial behavior of the reconstructed TPMD in p space. In order to examine the tangential resolution of the reconstruction of the TPMD we show in Fig. 5 plots of $\rho_{re}(\mathbf{p})$ and $\rho_{rt}(\mathbf{p})$ along a line parallel to [010] but located at a distance of $p=1.34$ a.u. from the origin in the (001) plane in $\mathbf{p}$ space. The gross features (viz., central peak, shoulders with steep decline, side peaks, etc.) observed in the experimental and theoretical curves match surprisingly well. As noticed previously, the structure in the theoretical curve appears exaggerated. Results shown in Fig. 5 indicate that the tangential resolution in the present reconstruction calculation at the radial distances in Fig. 5 is of the order of 0.15 a.u. (or 1.0 mrad) which matches well the 6° angular resolution mentioned earlier.

The results presented in Figs. 2–5 inspire us with a confidence that the present reconstruction scheme can reproduce structural details in the TPMD well within the expected statistical error and the radial and tangential resolutions. We shall now proceed to present our results in the form of 2D surfaces $\rho_{re}(p_x,p_y)$ in some interesting planes and compare them with the corresponding theoretical (without reconstruction) surfaces $\rho_t(p_x,p_y)$. As a typical illustration of the wealth of information provided by the reconstructed surfaces, $\rho_{re}(p_x,p_y)$, we have chosen three (p_x,p_y) planes passing through Γ ($p_z=0$), $\Gamma H/2$ ($p_z=\pi/a$), and H ($p_z=2\pi/a$); that is, (001) planes translated along [001].

A comparison of the experimental and theoretical surfaces of TPMD in the (001) plane passing through $p_z=0$ is shown in Fig. 6, where the relevant plane in the first BZ is shown in the inset. Examination of Fig. 6 shows that several structures observed in the theoretical surfaces are well reproduced by the reconstructed surface, $\rho_{re}(p_x,p_y)$, although with less sharpness. One prominent structure observed in Fig. 6 is the presence of hollows along ⟨110⟩ which arise from the NCE sheets of the FS as confirmed by the values of p_x and p_y at which they are observed. Another important structure observed in Fig. 6 is the steep decline in the second BZ and it is ascribed to the GCO and JGA hole sheets centered at Γ which cut along the ⟨110⟩ directions in the plane of Fig. 6. The effects of these three sheets of FS of V are brought out more prominently in Fig. 7 where we have shown a contour plot of the $\rho_{re}(p_x,p_y)$ surface of Fig. 6 in the relevant (p_x,p_y) plane. The regions where the different sheets of FS manifest themselves are marked by their labels (viz., NCE, GCO, and JGA).

Plots of $\rho_t(p_x,p_y)$ and $\rho_{re}(p_x,p_y)$ in the (001) plane which is displaced along $p_z=[001]$ by an amount π/a from the origin are compared in Fig. 8. In this plane the NCE's are positioned along the ⟨100⟩ directions and their presence is confirmed by the deep hollow structures observed in $\rho_{re}(p_x,p_y)$ along ⟨100⟩ and centered around 0.55 a.u. The presence of JGA is indicated by the hollow structures observed around 1.0 a.u. along ⟨100⟩ and around 1.4 a.u. along ⟨110⟩. A contour plot of this $\rho_{re}(p_x,p_y)$ surface (Fig. 8) is shown in Fig. 9 and these contours bring out the effects of FS topology more clearly.

In order to examine the TPMD reconstructed in a

plane further removed from the origin, we have compared in Fig. 10 the two surfaces $\rho_t(p_x,p_y)$ and $\rho_{re}(p_x,p_y)$ in a (001) plane, which is displaced along $p_z([001])$ by an amount $2\pi/a$ from the origin. These surfaces are lying in the second BZ and hence their amplitudes are expected to be small. Nevertheless, the general magnitude of $\rho_{re}(p_x,p_y)$ is in good agreement with the overall cloverleaf-shaped structure seen in $\rho_t(p_x,p_y)$ (Fig. 10). Examination of the FS topology reveals that the depression observed around the origin, $p_x=p_y=0$, in the $\rho_t(p_x,p_y)$ surface arises out of the JGA's cutting through this (p_x,p_y) plane. It is interesting to observe that corresponding depression is not seen in the $\rho_{re}(p_x,p_y)$ surface around the origin. The absence of the depression may be caused by the deenhancement of the surrounding $\rho(\mathbf{p})$ values since these result from the third band which is strongly of d character. Further studies are required to determine whether this is in fact the case.

The technique of 2D ACPAR measurements is capable of calipering the FS sheets in metals and this has been illustrated by applying the Lock-Crips-West theorem[34] to fold the $n^R(p_x,p_y)$ data from p space to k space. This has already been accomplished for V.[5,23] We feel that the $\rho_{re}(\mathbf{p})$ data reconstruction in the present work can be similarly folded back into the first BZ to obtain $\rho_{re}(\mathbf{k})$ which can lead to a determination of the FS or occupation number of electrons in k space.[1,2] Our previous work[23] has shown that the analysis of 2D ACPAR curves in p space itself can bring out interesting details of the FS of V. In order to demonstrate the usefulness of the reconstructed TPMD for mapping the FS topology we obtained $\rho_{re}(\mathbf{p})$ in a plane lying in the *HPHP* plane centered at *N* of the first BZ. A contour plot of $\rho_{re}(\mathbf{p})$ in this plane is shown in Fig. 11 where the relevant plane, symmetry points, and directions are shown in the inset. This plane is ideally suited to bring out the cross section of the NCE in the *HPN* plane. In addition, this plane is normal to the radial direction out from the origin and any distortion arising out of the slope of $\rho(\mathbf{p})$ should be small. The shape of the contours in Fig. 11 clearly bring out the elliptical cross section of the NCE. Although the contours do not allow an absolute measurement of the semiaxes of NCE along *NP* and *NH*, a determination of the ratio $(\overline{NP}/\overline{NH})$ of the semiaxes is possible. Such an analysis of Fig. 11 yields a ratio $\overline{NP}/\overline{NH}=1.36$ which compares satisfactorily (to within 7%) with the ratio of 1.27 determined experimentally by Phillips[35] (using the technique of impulsive fields) and Parker and Halloran[36] (using magnetothermal oscillation technique). It may be pointed out that the value $\overline{NP}/\overline{NH}=1.36$ determined by us is insensitive to the choice of contour used.

In the above we have presented reconstructed $\rho_{re}(\mathbf{p})$ along four directions and $\rho_{re}(p_x,p_y)$ in four planes in order to illustrate the usefulness of the present reconstruction scheme. In principle, one can extend this presentation of any direction or plane in the momentum space to examine the effect of the different sheets of FS on the TPMD. The reconstruction of TPMD from 2D ACPAR data sets is thus capable of bringing out rich details of TPMD (and therefore of the wave functions of electrons and positron) and FS in metals.

Recently it has been shown that the Fourier transform of TPMD, $B^{2\gamma}(\mathbf{r})$, provides a sensitive and useful quantity to compare experiment with theory.[1,37] We wish to point out that our reconstruction procedure leads to a calculation of $B^{2\gamma}(\mathbf{r})$ at an intermediate stage and although we have not presented these results here, we feel that such a possibility is another advantage of the present scheme of reconstructing TPMD.

V. CONCLUSIONS

The results presented in the preceding section show that a wealth of qualitative as well as quantitative information about the TPMD, $\rho(\mathbf{p})$, in $3d$ transition metals can be derived satisfactorily by applying the present reconstruction scheme to experimental 2D ACPAR data. It has been shown that the dimensions of the FS sheets can be determined by suitable analysis of the reconstructed TPMD. The results of the reconstruction are understood better if one applies the reconstruction method both to experimental data and theoretically generated data and compares the results with the theoretical TPMD. Our analysis also illustrates how the results of reconstruction can be understood in terms of the electronic band structure and FS topology in spite of the approximate nature of our band-structure calculations. Using a more accurate method of calculating TPMD and inclusion of e^+-e^- many-body correlations and combining such theory with a reconstruction method can lead us to a better understanding of the process of positron annihilation in metals. The results of reconstruction can be extended to obtain $B^{2\gamma}(\mathbf{r})$ and $\rho(\mathbf{k})$ and the latter can lead to determination of FS dimensions.

As far as the success of the reconstruction method is concerned, the present results show that for $3d$ metals with cubic structure it is possible to reach $l_{\max}=20-25$ in Eq. (3) using data sets, $n^R(p_x,p_y)$, for four p_z directions. Further work is necessary to determine which particular orientations should be chosen in a 2D ACPAR experiment so that high-quality reconstruction can be achieved from a limited set of data sets $n^R(p_x,p_y)$.

ACKNOWLEDGMENTS

Two of us (L.M.P. and R.M.S.) are grateful to the University of Geneva for their kind hospitality. We thank Dr. Rajendra Prasad for valuable suggestions. Part of this work was supported by the U.S. Office of Naval Research and by the Swiss National Science Foundation.

[1]S. Berko, in *Positron Solid State Physics,* edited by W. Brandt and A. Dupasquier (North-Holland, Amsterdam, 1983).

[2]R. N. West, in *Positron Annihilation,* edited by P. C. Jain, R. M. Singru, and K. P. Gopinathan (World-Scientific, Singapore, 1985), p. 11.

[3]P. E. Mijnarends, in *Positron Solid State Physics,* edited by W. Brandt and A. Dupasquier (North-Holland, Amsterdam, 1983).

[4]R. M. Singru, in *Positron Annihilation,* edited by P. G. Coleman, S. C. Sharma, and L. M. Diana (North-Holland, Amsterdam, 1982).

[5]A. A. Manuel, Phys. Rev. Lett. **49**, 1525 (1982); T. Jarlborg, A. A. Manuel, and M. Peter, Phys. Rev. B **27**, 4210 (1983).

[6]*Image Reconstruction from Projections,* edited by G. T. Herman (Springer-Verlag, Berlin, 1979); R. A. Brooks and G. Di-Chiro, Phys. Med. Bio. **21**, 689 (1976).

[7]P. E. Mijnarends, in *Compton Scattering,* edited by B. Williams (McGraw-Hill, New York, 1977), p. 323.

[8]P. E. Mijnarends, Phys. Rev. **160**, 512 (1967); **178**, 622 (1969).

[9]F. M. Mueller, Phys. Rev. B **15**, 3039 (1977).

[10]N. K. Hamsen, P. Pattison, and J. R. Schneider, Z. Phys. B **66**, 305 (1987); N. K. Hansen, Hahn-Meitner-Institut Report No. HMI-B-342, 1980 (unpublished); P. Pattison, N. K. Hansen, and J. R. Schneider, Chem. Phys. **59**, 231 (1981).

[11]E. Heuser-Hofmann and W. Weyrich, Z. Naturforsch. **40a**, 99 (1985).

[12]C. K. Majumdar, Phys. Rev. B **4**, 2111 (1971).

[13]M. R. Howells and P. E. Osmon, J. Phys. F **2**, 277 (1972).

[14]F. Sinclair, W. S. Farmer, and S. Berko, in *Positron Annihilation,* edited by P. G. Coleman, S. C. Sharma, and L. M. Diana (North-Holland, Amsterdam, 1982), p. 322.

[15]R. L. Waspe and R. N. West, in *Positron Annihilation,* edited by P. G. Coleman, S. C. Sharma, and L. M. Diana (North-Holland, Amsterdam, 1982), p. 328; K. R. Hoffman, S. Berko, and B. J. Bequdy, *ibid.*, p. 325.

[16]A. M. Cormack, J. Appl. Phys. **34**, 2722 (1963); **35**, 2908 (1964).

[17]L. Pecora and A. C. Ehrlich, Phys. Rev. B **19**, 719 (1979); L. M. Pecora and A. C. Ehrlich, Phys. Rev. Lett. **46**, 1476 (1981); Phys. Rev. B **32**, 708 (1985).

[18]G. Kontrym-Sznajd, in *Positron Annihilation,* edited by P. G. Coleman, S. C. Sharma, and L. M. Diana (North-Holland, Amsterdam, 1982), p. 346.

[19]S. Daniuk, G. Kontrym-Sznajd, J. Mayers, A. Rubazek, H. Stachowiak, P. A. Walters, and R. N. West, in *Positron Annihilation,* edited by P. C. Jain, R. M. Singru, and K. P. Gopinathan (World-Scientific, Singapore, 1985), p. 279.

[20]L. M. Pecora, IEEE Trans. Nucl. Sci. **NS-34**, 642 (1987).

[21]L. M. Pecora, A. C. Ehrlich, A. A. Manuel, A. K. Singh, and R. M. Singru, in *Positron Annihilation,* edited by P. C. Jain, R. M. Singru, and K. P. Gopinathan (World-Scientific, Singapore, 1985), p. 254.

[22]A. K. Singh and R. M. Singru, J. Phys. F **12**, 685 (1982); A. K. Singh, Ph.D. thesis, Indian Institute of Technology, Kanpur, 1981 (unpublished).

[23]A. K. Singh, A. A. Manuel, R. M. Singru, R. Sachot, E. Walker, P. Descouts, and M. Peter, J. Phys. F **15**, 2375 (1985); R. M. Singru, A. A. Manuel, A. K. Singh, R. Sachot, E. Walker, P. Descouts, and M. Peter, in *Positron Annihilation,* edited by P. C. Jain, R. M. Singru, and K. P. Gopinathan (World-Scientific, Singapore, 1985), p. 269.

[24]S. L. Altmann, Proc. Cambridge Philos. Soc. **53**, 343 (1957); S. L. Altmann, Philos. Trans. R. Soc. London, Ser. A **255**, 199 (1963); S. L. Altmann and A. P. Cracknell, Rev. Mod. Phys. **37**, 19 (1965); S. L. Altmann and C. J. Bradley, *ibid.* **37**, 33 (1965).

[25]P. E. Bisson, P. Descouts, A. Dupanloup, A. A. Manuel, E. Perreard, M. Peter, and R. Sachot, Helv. Phys. Acta **55**, 100 (1982).

[26]J. Hubbard, J. Phys. C **2**, 1222 (1969); J. Hubbard and P. E. Mijnarends, *ibid.* **5**, 2323 (1972).

[27]P. E. Mijnarends, Physica Utrecht **63**, 235 (1973).

[28]D. G. Kanhere and R. M. Singru, J. Phys. F **7**, 2603 (1977).

[29]A. K. Singh, A. A. Manuel, T. Jarlborg, Y. Mathys, E. Walker, and M. Peter, Helv. Phys. Acta **59**, 410 (1986).

[30]V. L. Moruzzi, J. F. Janak, and A. R. Williams, *Calculated Electronic Properties of Metals* (Pergamon, Oxford, 1978).

[31]A. K. Singh and T. Jarlborg (private communication).

[32]P. E. Mijnarends and R. M. Singru, Phys. Rev. B **19**, 6038 (1979).

[33]M. Sob, J. Phys. F **12**, 571 (1982).

[34]D. G. Lock, V. H. C. Crisp, and R. N. West, J. Phys. F **3**, 561 (1973); D. G. Lock and R. N. West, Appl. Phys. **6**, 249 (1975); G. M. Beardsley, S. Berko, J. J. Mader, and M. A. Schulman, *ibid.* **5**, 375 (1975).

[35]R. A. Phillips, Phys. Lett. **36A**, 361 (1971).

[36]R. D. Parker and M. M. Halloran, Phys. Rev. B **9**, 4130 (1974).

[37]A. K. Singh, A. A. Manuel, R. M. Singru, and M. Peter, Helv. Phys. Acta **58**, 640 (1985); A. K. Singh, A. A. Manuel, R. M. Singru, T. Jarlborg, A. Vanuzzio, and M. Peter, in *Positron Annihilation,* edited by P. C. Jain, R. M. Singru, and K. P. Gopinathan (World-Scientific, Singapore, 1985), p. 273.

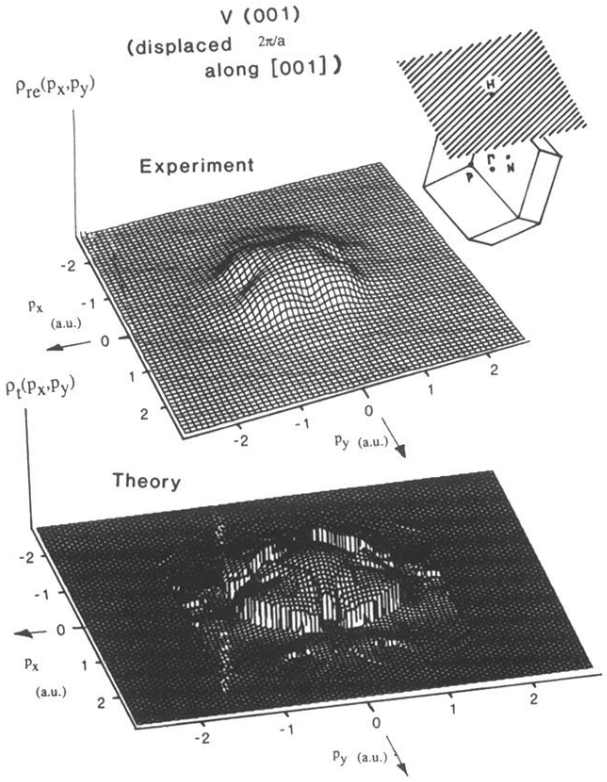

FIG. 10. Same as Fig. 6, but for a $(p_x,p_y)=(001)$ plane situated at $p_z=2\pi/a$ along the [001] direction.

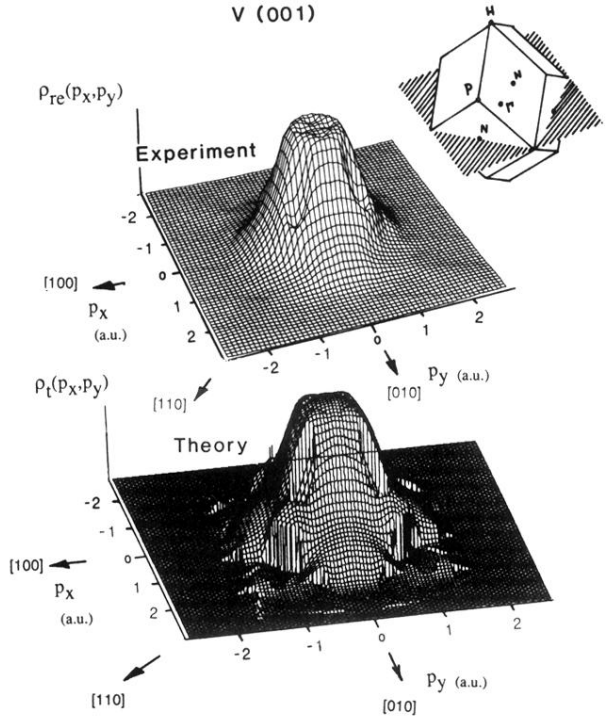

FIG. 6. The TPMD surfaces $\rho_t(p_x,p_y)$ and $\rho_{re}(p_x,p_y)$ (see text) in the $(p_x,p_y)=(001)$ plane passing through Γ at $p_z=0$. The particular (p_x,p_y) plane is shown in the inset at the top right corner.

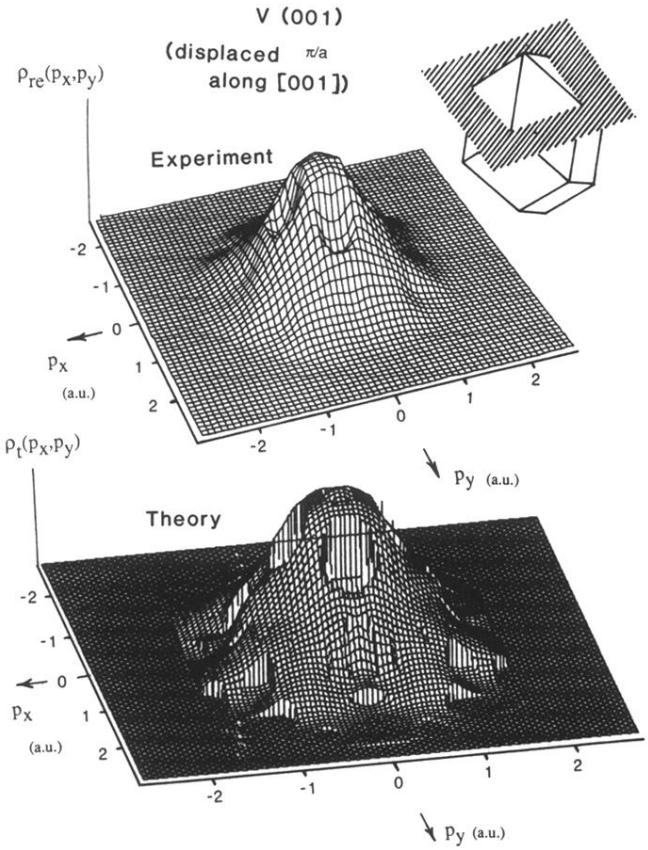

FIG. 8. Same as Fig. 6, but for $(p_x,p_y)=(001)$ situated at $p_z=\pi/a$ along the [001] direction.